Combustion-Relevant Temperature Imaging with Scattering Referenced Aerosol Phosphor Thermometry Applied to Eu:BAM

Dustin Witkowski, Joshua M. Herzog, David A. Rothamer

University of Wisconsin-Madison, 1500 Engineering Dr., Madison, WI 53706

Abstract

This work demonstrates precise aerosol phosphor thermometry (APT) measurements over a large temperature range by applying scattering-referenced APT (SRAPT) with the phosphor divalent Europium doped in Barium Magnesium Aluminate (Eu:BAM). Measurements were taken using Eu:BAM seeded into an air jet mixing with the products of a concentric methane-air flat flame. In-situ calibration of the SRAPT ratio versus temperature was performed from 500-1400 K. Peak temperature sensitivities of 1-1.5 %/K were observed, approximately 4 times higher than the spectral luminescence intensity ratio method typically used for Eu:BAM. Despite its moderate quenching temperature (700 K), the high initial signal intensities before the onset of thermal quenching for Eu:BAM allowed reliable single-shot measurements to be made continuously from 500 K to greater than 1200 K. These results highlight the importance of high signal levels for extending the measurement range of SRAPT.

Keywords: Aerosol phosphor thermometry, Thermographic phosphors, Thermal quenching

Preprint submitted to Combustion and Flame *October 31, 2020*

1. Introduction

Aerosol phosphor thermometry (APT) is a laser-based temperature imaging technique that relies on the emission properties of thermographic phosphor particles seeded into a flow to make planar gas temperature measurements. Upon capturing elastic laser scattering from the particles, simultaneous particle image velocimetry (PIV) measurements can be performed, making APT a promising diagnostic for the study of turbulent reacting environments. One of the most used phosphors for APT has been divalent Europium doped in Barium Magnesium Aluminate (Eu:BAM) [1, 2, 3, 4, 5, 6, 7]. Eu:BAM has high room-temperature signal levels and can be efficiently excited with both 266- and 355-nm sources [3, 8]. This has enabled precise APT measurements from room temperature up to approximately 700 K with the spectral luminescence intensity ratio (SLIR) approach [2]. Unfortunately, simultaneously decreasing spectral temperature sensitivity and signal with increasing temperature has limited SLIR measurements with Eu:BAM to temperatures less than 1000 K [3, 7].

Scattering-referenced APT (SRAPT) has recently been employed to extend the temperature range of accurate single-shot APT measurements [9, 10, 11]. SRAPT relies on the temperature sensitivity of the phosphor's emission intensity. Above a threshold temperature, excited phosphor emission begins decreasing rapidly due to increasing nonradiative transition rates (thermal quenching). The high sensitivity associated with this rapid decrease can be used for single-shot temperature imaging until signal levels drop too low to be measured with a sufficient signal-to-noise ratio (SNR). To date, the phosphors used for SRAPT have been excited at non-optimal wavelengths with relatively low ground state absorption cross sections. This leads to low initial signal levels prior to the onset of thermal quenching, and has limited the dynamic range of the measurement technique generally to a few hundred kelvins after the onset of thermal quenching.

The current work takes advantage of Eu:BAM's high pre-quenching signal levels to extend the temperature measurement range with Eu:BAM to beyond

1000 K by utilizing SRAPT. Background into SRAPT and factors governing its' performance at high temperatures are discussed. Measurements performed in a seeded air jet mixed with the products of a methane-air flat flame are presented. Single-shot and average temperature profiles are compared to thermocouple measurements and are used to assess the viability of Eu:BAM SRAPT for combustion-relevant temperature imaging.

2. Diagnostic Background

SRAPT measurements are performed by taking the ratio of temperature-insensitive per particle Mie scattering signal (S_{Mie}) to temperature-dependent luminescence signal (S_{Lum}) emitted from phosphor particles. For Eu^{2+} the temperature dependence of the luminescence intensity is the result of thermal quenching caused by ionization of excited electrons to the conduction band, and can be approximated by [12]

$$S_{\mathrm{Lum}} = \frac{S_i}{1 + C_{\mathrm{NR}} \exp\left(- \frac{E_{\mathrm{dc}}}{k_B T} \right)}, \tag{1}$$

where S_i is the signal intensity prior to the onset of thermal quenching, C_{NR} is a temperature-independent ratio of the electronic nonradiative and radiative transition probabilities, E_{dc} is the energy gap between the lowest 5d level and the bottom of the host conduction band and k_{B} is the Boltzmann constant. Assuming negligible temperature-dependence in S_i (i.e., no significant change in absorption cross section with temperature), the SRAPT ratio can be written as

$$R = \frac{S_{\mathrm{Mie}}}{S_{\mathrm{Lum}}} \propto 1 + C_{\mathrm{NR}} \exp\left(- \frac{E_{\mathrm{dc}}}{k_B T} \right). \tag{2}$$

The temperature precision index (standard deviation) of a ratio-based technique like SRAPT is given by

$$s_T = \frac{s_R}{R} \frac{1}{\xi_T}, \tag{3}$$

where s_R is the single-shot precision index for the ratio, and the fractional temperature sensitivity is defined as

$$\xi_T = \frac{1}{R}\frac{\partial R}{\partial T}. \tag{4}$$

For SRAPT measurements, it has been previously shown [11] that the fractional ratio precision in the shot-noise limit can be written as

$$\frac{s_R}{R} = \sqrt{\frac{K_1}{S_{\mathrm{Mie}}} + \frac{K_2}{S_{\mathrm{Lum}}}} = \frac{1}{\sqrt{S_{\mathrm{Lum}}}}\sqrt{\frac{K_1}{R} + K_2}, \tag{5}$$

where K_1 accounts for noise from the scattering camera and an added contribution due to differing dependencies of scattering and luminescence on particle size, and K_2 accounts for noise in the luminescence camera. This work focuses on making measurements at high temperatures well past the onset of thermal quenching, such that $R >> 1$. In this limit, using the result of equation 1, equation 5 can be re-written as

$$\frac{s_R}{R} \propto \frac{1}{\sqrt{S_i}} \exp\left(-\frac{E_{\mathrm{dc}}}{2k_bT}\right). \tag{6}$$

Similarly, the fractional temperature sensitivity for large ratios is given by

$$\xi_T \propto \frac{E_{\mathrm{dc}}}{T^2}, \tag{7}$$

and equation 3 can thus be written in a convenient form

$$s_T \propto \frac{T^2}{E_{\mathrm{dc}}} \frac{\exp\left(-\frac{E_{\mathrm{dc}}}{2k_bT}\right)}{\sqrt{S_i}}, \quad \text{for } R >> 1. \tag{8}$$

Equation 8 highlights two characteristics that make a thermographic phosphor useful for SRAPT at high temperatures: a large energy gap for thermal quenching and high pre-quenching signal levels.

Figure 1 compares the signal per particle volume versus temperature for Eu:BAM and for Ce^{3+} emission from the Ce,Pr:LuAG phosphor. The measurements were taken previously in a tube furnace [9, 13], and the absolute magnitude was determined from previously reported values of each phosphor's room temperature per particle signal intensity at a fluence of 20 mJ/cm^2 [8, 14].

The Ce,Pr:LuAG phosphor has recently been shown to be capable of making precise measurements employing SRAPT using Ce^{3+} emission from 700 – 1000 K [9, 10]. At higher temperatures, its signal becomes too low to be usable for single-shot imaging measurements with the equipment and excitation wavelength used in that work. In contrast, Eu:BAM signal per particle volume at room temperature is approximately 2 orders of magnitude brighter, and still has signal intensities higher than Ce,Pr:LuAG's room-temperature emission at temperatures above 1000 K. Therefore, despite the fact that both of these phosphors quench at similar temperatures (i.e., similar values of E_{dc}), temperature measurements with Eu:BAM should be achievable at much higher SRAPT ratios (for the same imaging spatial resolution), enabling measurements at significantly higher temperatures.

3. Experimental Setup

Measurements were performed in a 12-mm inner diameter air jet seeded with Eu:BAM particles (Phosphor Technology, 1.1 μm diameter by volume based on in-house electrical low pressure impactor (ELPI, Dekati) measurements) that entrained hot combustion products from the surrounding concentric flat flame burner (Holthius and Associates center-tube burner), as shown in Figure 2. The measured flowrate of the seeded jet was 2.0 SLPM (Alicat M-50SLPM), corresponding to a laminar Reynolds number of 230 at the jet exit. The surrounding flat methane/air flame had an outside diameter of 60 mm and was operated at an equivalence ratio of 1.1 (CH4 flowrate = 5.6 SLPM, Alicat M-10SLPM; Air flowrate = 49.3 SLPM, Alicat M-100SLPM). As a result of the jet mixing with the flame products, the jet gas that was originally at room temperature was heated to temperatures approaching the flame temperature far above the burner surface.

The experimental setup used for the jet imaging measurements is shown in Figure 3. The third harmonic output of a 10-Hz Nd:YAG laser (Continuum Powerlite 8010, 355 nm) was formed into a 50-mm tall by 0.7-mm thick laser

sheet using the combination of a -75-mm FL cylindrical lens and a 500-mm FL spherical lens. Excitation at 355 nm results in efficient absorption by Eu^{2+} ions in BAM, as it is near the peak of its' excitation spectrum [15]. The measured mean fluence was 30 ± 3 mJ/cm^2.

One intensified ICCD camera (Princeton Instruments PI-MAX 2) was used to measure elastic scattering of laser light from the phosphor particles (Mie camera) and a second ICCD camera (Princeton Instruments PI-MAX 4) was used to measure the Eu:BAM luminescence intensity (Lum. camera). The Mie camera was outfitted with a 45-mm $f/1.8$ UV camera lens (Sodern Cerco 2073) and a 355-nm bandpass filter (Edmund Optics 67-893) to collect the elastic scattering, whereas the luminescence camera utilized a 50-mm $f/1.2$ manual focus lens (Nikon Nikkor) in combination with a 355-nm longpass filter (Semrock BLP01-355R) and a 490-nm shortpass filter (Asahi Spectra ZVS0490) to collect the Eu:BAM luminescence. A room temperature emission spectrum for Eu:BAM measured in previous work [13] is shown in Figure 4 with the collection band used for the imaging experiments superimposed. The Mie camera was operated with its lens stepped down near its minimum aperture size ($f/32$) so signal levels were low enough to ensure a linear intensifier response [11], while the luminescence camera had its lens completely opened ($f/1.2$) to maximize the luminescence intensity and thus the dynamic range of the measurement.

Both cameras began gating 10 ns prior to the laser pulse. A gate width of 2 μs was used to collect the luminescence emission and a 100 ns gate width was used for collection of the laser scattering. No hardware binning was performed on the luminescence camera due to the high room-temperature signal levels, whereas the Mie camera was hardware binned 2x2. Each image was software binned following background subtraction to a final pixel size of 0.495 mm, corresponding to 6 binned pixels and an image magnification of $M = 0.154$. The spatial resolution for each camera was determined using a binned 1951 USAF target placed at the location of the laser sheet on top of the burner. The image contrast transfer function ($C = (I_{\max} - I_{\min})/(I_{\max} + I_{\min})$, $I_{\max}$ = Maximum intensity of line pattern and $I_{\min}$ = Minimum intensity of line pattern) was 0.6 for Group

0, Element 1 on the luminescence camera and Group 0, Element 2 on the Mie camera, corresponding to a resolution of 1-1.12 lp/mm, or approximately 2 binned camera pixels for the imaging experiment.

Due to the high signal intensities (∼40,000 un-binned counts out of 65536, 16-bit) measured on the luminescence camera, a correction was performed to account for nonlinearity in the camera intensifier response, as has been done previously [11, 16]. This was performed by comparing the measured signal intensities on both the luminescence and Mie cameras in a regime where it has been previously established that the Mie camera is linear with respect to incident photon flux [11]. Both the raw data and linearity correction are shown in Figure 5.

After linearizing the luminescence camera, the SRAPT ratio was formed and whitefield corrected. Finally, a threshold was implemented to account for background variation and noise. This excludes pixels with insufficient phosphor seeding density. A value of 1000 counts on the Mie scattering camera (prior to software binning) was used to ensure seeding densities greater than approximately 100 mm^{-3} (see next paragraph). A value of 100 counts prior to software binning was used for the luminescence camera as a tradeoff between maximizing the dynamic range of the measurement (i.e., using the entire range of the camera) and attempting to stay within the range where the camera response is approximately linear at low signals.

The Mie camera was calibrated to calculate seeding density for each single-shot image (n_p) using luminescence intensity per mass data from [8] in combination with imaging and experimental specifications. First, seeding density was calculated on the luminescence camera at room temperature using the following expression

$$n_p = \frac{S_{\text{corr}}}{V_{pix} m_p S_m \frac{\Omega}{4\pi} \eta_{\text{coll}} G}. \tag{9}$$

In equation 9, S_{corr} is the measured luminescence intensity (in un-binned counts) corrected for linearity in camera counts, and all other terms are defined in Table 1. The measured photons emitted per phosphor mass (S_m) was taken from pre-

Table 1: Experimental parameters used to calibrate scattering camera for estimation of single-shot seeding density fields.

Symbol	Definition	Value	Units
G	System gain	150	[counts/e$^-$]
η_{coll}	Product of average photocathode and optical efficiency	0.31	[e$^-$/photon]
$\Omega/4\pi$	Luminescence camera collection solid angle	7.73E-4	[-]
V_{pix}	Un-binned pixel volume	0.0048	[mm^3]
S_m	Photons emitted per phosphor mass	4.3E5	[photon/pg]
m_p	Average mass per particle	2.44	[pg]

vious work [8] and adjusted to account for both the fact that the luminescence camera is only collecting one lifetime worth of emission at room temperature and for the difference in fluence between experiments using previously published Eu:BAM room temperature fluence curves [3]. Finally, a linear relationship between the scattering camera's signal intensity and the seeding density measured by the luminescence camera was established at room temperature and used to provide single-shot seeding density field measurements in the heated jet, assuming negligible temperature-dependence in per particle scattering intensity.

Calibration of the measurements to temperature was performed by comparing the measured mean ratio along the axis of the jet against fine wire type-R thermocouple measurements and previous measurements in the same setup using the Ce,Pr:LuAG phosphor. Both the phosphor and thermocouple measurements are reported elsewhere [10]. The measured thermocouple temperatures were corrected for both radiation and conduction using heat transfer and material property correlations from [17]. Three horizontal sweeps were acquired with a 0.127-mm diameter wire thermocouple at heights above the burner (HABs) of 24, 37, and 48 mm. The temperature derivatives along the wire needed to estimate conduction error were determined directly from the horizontal profiles. The estimated conduction error correction along the jet centerline varied from approximately 200 K at 600 K to less than 15 K at 1000 K. Due to the large re-

quired thermocouple conduction corrections below 1000 K, measurements using Ce,Pr:LuAG [10] in the same setup were used for calibration over this range. Above 1000 K (>40 mm HAB) the measured ratio was compared to a vertical profile taken using a 0.0762-mm diameter Type-R thermocouple, which was corrected for radiation but not conduction, as conduction error was estimated to be <15 K for these locations. The radiation error correction magnitude was found to vary from less than 10 K at 1050 K to a maximum of 60 K at 1600 K.

4. Experimental Results

Figure 6a shows in situ measurements of the SRAPT ratio for Eu:BAM as a function of temperature. The results are compared to furnace measurements of Eu:BAM in bulk powder form [13]. For these measurements it is assumed that the SRAPT ratio temperature dependence in the furnace is equal to the inverse of the luminescence intensity, normalized by its room temperature value (i.e., $R = S_{\mathrm{Lum}}(300\ \mathrm{K})/S_{\mathrm{Lum}}(T)$). To make the measurements directly comparable, the furnace measurements were corrected to account for the 2 μs gate width used in the flame experiments. This was accomplished by supplementing the total signal versus temperature curves measured in the furnace with lifetime data of Eu:BAM up to 1100 K previously reported in the literature [18], using the following relationship for single-exponential time decays

$$S_{t_g,Lum} = S_{\mathrm{tot}}(1 - \exp(-t_g/\tau)). \tag{10}$$

In equation 10, S_{tot} is the total integrated signal measured in the tube furnace, $S_{t_g,Lum}$ is the total integrated signal measured at time t_g after the laser pulse ($t_g = 2\ \mu s$, corresponding to the gate width used) and τ is the emission lifetime of Eu:BAM as a function of temperature [18].

The thermal quenching behavior is apparent in Figure 6a in both experiments as the rapid increase in the SRAPT ratio once the onset of thermal quenching occurs. The behavior for both the jet and furnace measurements is similar, although there are differences in behavior at lower temperatures. The

onset of quenching appears to occur approximately 50 K earlier in the jet. This may be a result of particle heating at the higher laser fluences used in the jet measurements [3, 13], bulk scattering effects in the furnace affecting absorption temperature-dependencies, or uncaptured biases in the thermocouple measurements used for the in-situ calibration. The earlier quenching in the jet relative to the furnace environment has been observed for Eu:BAM in other experiments [5].

Figure 6b displays the measured fractional sensitivity of the technique (defined by equation 4), both for the in-situ calibration and furnace measurements. For the furnace measurements, a cubic spline interpolation of the ratio versus temperature was performed prior to taking its derivative. This gave the sensitivity curve a smoother appearance. Employing the SRAPT technique with Eu:BAM leads to high peak sensitivities, approximately 1-1.5 %/K. The peaks are offset in temperature by ∼35 K for the jet and furnace measurements. Reasonably high temperature sensitivity is also observed prior to the onset of quenching ($T < 700$ K). This may be due to a decreasing absorption cross section with increasing temperature.

As temperature increases above 1000 K and the ratio becomes large, the sensitivity begins dropping relatively quickly as expected based on equation 7. Even with this decrease, the sensitivity is still ∼0.4 %/K at 1200 K. In comparison, the maximum typical temperature sensitivity for Eu:BAM with the SLIR technique occurs at room temperature, and is only ∼0.3 %/K. By 900 K, this value has already dropped to well below 0.1 %/K [3].

The calibration for thermometry employed a double exponential fit to the temperature versus SRAPT ratio. The selected calibration form was chosen solely for the purpose of establishing an analytical relationship that matched the data well; the results are provided in Figure 7. The maximum residual between the fit and data is 2-3 % between 800 and 870 K, and less than 2 % over the entire rest of the range from 500 – 1400 K.

Figures 8a and 8b display the average and a selected single-shot temperature image, respectively. The full array of single-shot temperature images are

available in the supplemental information. In both images, the inward heating resulting from the jet mixing with flame products is apparent, and gives the temperature profile an appearance very similar to that of a diffusion flame. The seeding density for the selected single-shot image is also shown in Figure 8c. The seeding density is fairly high in the center of the jet, near the exit (1500 mm^{-3}), and then decreases significantly as the surrounding flame products are mixed in and the jet is heated.

Figure 9a compares the measured average and single-shot profile along the jet centerline (single pixel) to the measurements [10] used for the in-situ calibration as a means of investigating the range of temperatures the technique is capable of measuring. Reliable average measurements are achieved from 500 – 1400 K. Due to Eu:BAM's high signal levels, in combination with the 6x6 software binning, SRAPT ratios as high as ∼500 are measured with sufficient SNR to allow for temperature determination. While a quantitative assessment of measurement precision is not possible in the current setup due to slight unsteadiness in the jet, the smoothness of the single-shot profiles at temperatures up to ∼1200 K points to the potential for precise measurements above 1000 K using Eu:BAM with the SRAPT technique. A complete characterization of the technique in a more controlled environment is needed in the future to assess both precision and potential measurement biases as a function of laser fluence and seeding density.

Radial profiles are compared to thermocouple measurements at three different heights in Figure 9b. The SRAPT and thermocouple measurements agree reasonably well near the centerline of the jet at all heights. Some significant disagreement is seen at distances greater than 3 mm from the jet centerline, particularly at 24 mm above the burner surface. One factor likely contributing to this disagreement is the scattering of bright luminescence emitted from the cold jet core (which has a high number density of particles) by particles in the surrounding high temperature regions at the periphery of the jet, artificially increasing signal in the hot, low signal, regions and resulting in a temperature measurement bias. This observation is supported by the improved agreement with the thermocouple measurements observed higher in the flame, where seed-

ing densities are lower and there is a smaller temperature difference (i.e., signal difference) between the jet centerline and the periphery of the jet. Uncertainty in the thermocouple measurements may contribute to some of the disagreement observed as well, due to the large conduction corrections required in the presence of large temperature gradients. Similar to the centerline profiles, the single-shot radial profiles are very smooth until approximately 1200 K.

5. Conclusions

This work has demonstrated the ability to achieve measurements over large temperature ranges with the SRAPT technique by taking advantage of the high pre-quenching signal levels for Eu:BAM. Continuous measurements were demonstrated from 500 to 1400 K, more than 400 K higher than previously capable with Eu:BAM using the conventional spectral luminescence intensity ratio measurement technique. These results highlight the importance of high signal levels on phosphor performance, and should open up new avenues for APT to study turbulence-chemistry interactions in combustion processes.

6. Acknowledgements

Research was sponsored by the Army Research Office and was accomplished under Grant Number W911NF-19-1-0238. The views and conclusions contained in this document are those of the authors and should not be interpreted as representing the official policies, either expressed or implied, of the Army Research Office or the U.S. Government. The U.S. Government is authorized to reproduce and distribute reprints for Government purposes notwithstanding any copyright notation herein.

References

[1] C. Abram, B. Fond, A. L. Heyes, F. Beyrau, High-speed planar thermometry and velocimetry using thermographic phosphor particles, Appl. Phys. B 111 (2) (2013) 155–160.

[2] B. Fond, C. Abram, A. L. Heyes, A. M. Kempf, F. Beyrau, Simultaneous temperature, mixture fraction and velocity imaging in turbulent flows using thermographic phosphor tracer particles, Opt. Express 20 (20) (2012) 22118–22133.

[3] B. Fond, C. Abram, F. Beyrau, Characterisation of the luminescence properties of BAM: Eu2+ particles as a tracer for thermographic particle image velocimetry, Appl. Phys. B 121 (4) (2015) 495–509.

[4] H. Lee, B. Böhm, A. Sadiki, A. Dreizler, Turbulent heat flux measurement in a non-reacting round jet, using BAM: Eu2+, Appl. Phys. B 122 (7) (2016) 1–13.

[5] C. Abram, B. Fond, F. Beyrau, Temperature measurement techniques for gas and liquid flows using thermographic phosphor tracer particles, Prog. Energy Combust. Sci. 64 (Supplement C) (2018) 93–156. doi:https://doi.org/10.1016/j.pecs.2017.09.001.
URL http://www.sciencedirect.com/science/article/pii/S0360128516301654

[6] J. Linden, N. Takada, B. Johansson, M. Richter, M. Alden, Investigation of potential laser-induced heating effects when using thermographic phosphors for gas-phase thermometry, Appl. Phys. B 96 (2-3) (2009) 237–240. doi:10.1007/s00340-009-3608-7.
URL <GotoISI>://000267885000003

[7] Z. Yin, B. Fond, G. Eckel, C. Abram, W. Meier, I. Boxx, F. Beyrau, Investigation of BAM: Eu2+ particles as a tracer for temperature imaging in flames, Combust. Flame 184 (2017) 249–251.

[8] B. Fond, C. Abram, M. Pougin, F. Beyrau, Characterisation of dispersed phosphor particles for quantitative photoluminescence measurements, Opt. Mater 89 (2019) 615–622.

[9] D. Witkowski, J. Herzog, D. A. Rothamer, High-precision aerosol phosphor thermometry with Ce^{3+} and Pr^{3+} co-doped into lutetium aluminum garnet, in: 11th U.S. National Combustion Meeting, 2019.

[10] J. M. Herzog, D. Witkowski, D. A. Rothamer, Combustion-relevant aerosol phosphor thermometry imaging using Ce,Pr:LuAG, Ce:GdPO4, and Ce:CSSO, Proc. Combust. Inst.doi:https://doi.org/10.1016/j.proci.2020.06.193.

[11] D. Witkowski, D. A. Rothamer, Scattering referenced aerosol phosphor thermometry, Meas. Sci. Technol. 30 (4) (2019) 044003.

[12] P. Dorenbos, Thermal quenching of Eu2+ 5d–4f luminescence in inorganic compounds, J. Phys. Condens. Matter 17 (50) (2005) 8103.

[13] D. Witkowski, D. A. Rothamer, Investigation of aerosol phosphor thermometry (APT) measurement biases for Eu: BAM, Appl. Phys. B 124 (10) (2018) 202.

[14] J. M. Herzog, D. Witkowski, D. A. Rothamer, Characterization of the Ce,Pr:LuAG Phosphor for Co-doped Aerosol Phosphor Thermometry, In revision.

[15] T. Justel, Phosphor Information and Spectra Access (PISA) (2019 (accessed October 2, 2019)).
URL fh-muenster.de/ciw/personal/professoren/juestel/pisa.php

[16] T. C. Williams, C. R. Shaddix, Simultaneous correction of flat field and nonlinearity response of intensified charge-coupled devices, Rev. Sci. Instrum. 78 (12) (2007) 123702.

[17] V. Hindasageri, R. Vedula, S. Prabhu, Thermocouple error correction for measuring the flame temperature with determination of emissivity and heat transfer coefficient, Rev. Sci. Instrum. 84 (2) (2013) 024902.

[18] G. Sarner, M. Richter, M. Alden, Investigations of blue emitting phosphors for thermometry, Meas. Sci. Technol. 19 (12) (2008) 10. doi:12530410.1088/0957-0233/19/12/125304.
URL <GotoISI>://000260759000011

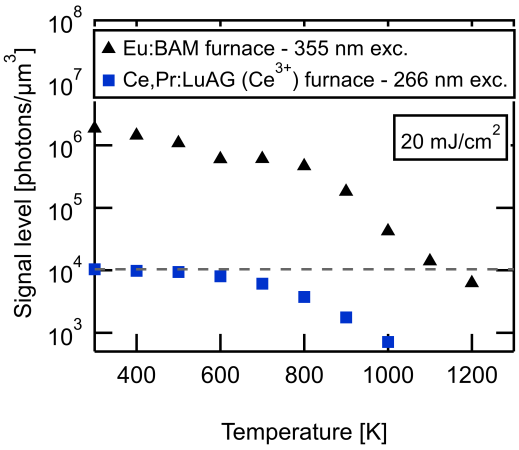

Figure 1: Signal per particle volume for Eu:BAM and Ce,Pr:LuAG as a function of temperature. The temperature-dependence of the signal was determined from tube furnace measurements [9, 13]. The absolute value of the signal intensity is based on room-temperature per particle signal measurements in a dispersed environment at 20 mJ/cm^2. Absolute intensity measurements were performed at 355 nm for Eu:BAM [8] and 266 nm for Ce,Pr:LuAG [14]

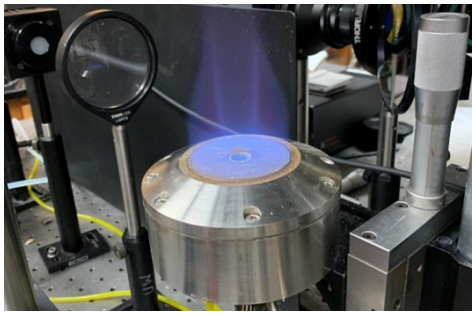

Figure 2: Center tube flat flame burner used for temperature imaging experiments. The center tube in the picture is where the air jet seeded with Eu:BAM particles exits, and then mixes with the products of the methane/air flame.

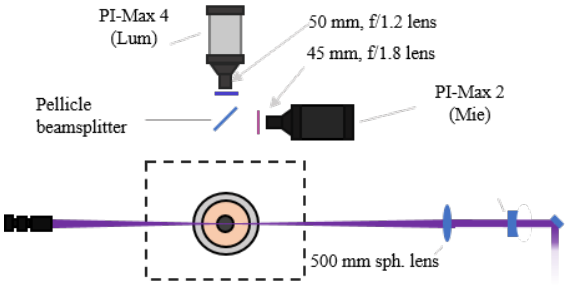

Figure 3: Experimental setup for flame imaging experiments.

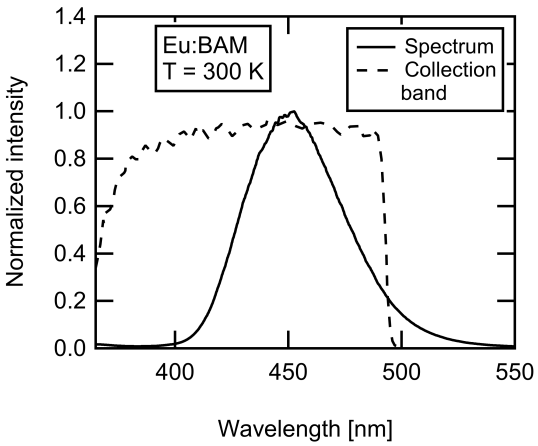

Figure 4: Measured emission spectrum of Eu:BAM at 300 K in solid line. The collection band used for the imaging experiment is shown as the dashed line.

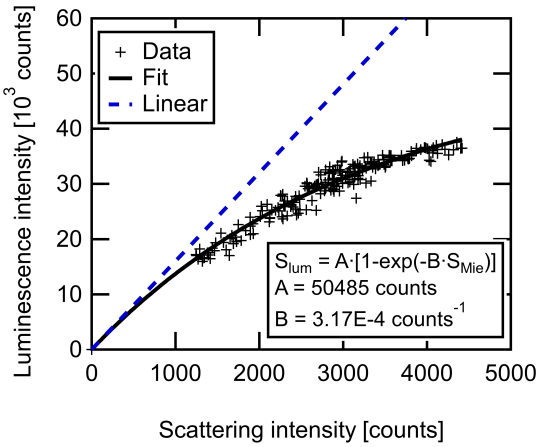

Figure 5: Measured luminescence intensity versus scattering intensity at room temperature. The black line represents a curve fit used to linearize the luminescence camera's response, and the blue dotted line shows the behavior expected for a linear intensifier response. The data used for the correction was averaged over a 4x7 mm region near the jet exit

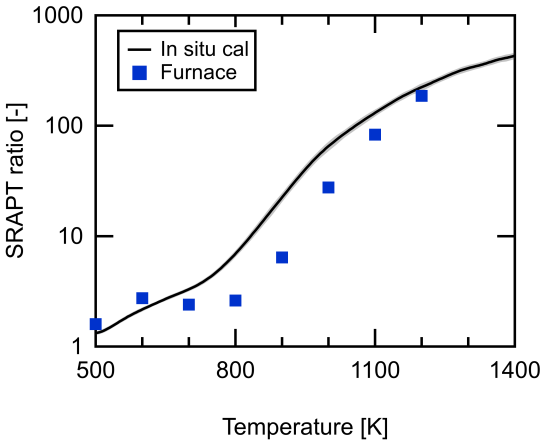

(a)

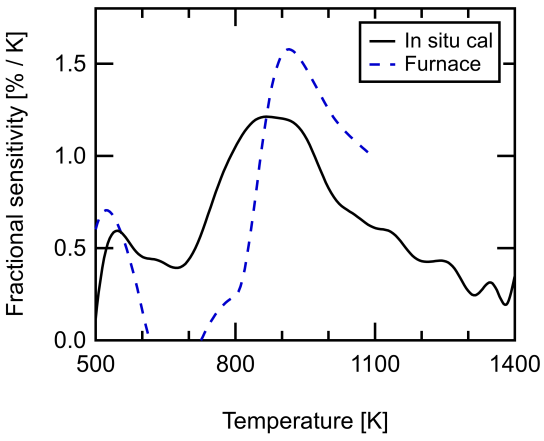

(b)

Figure 6: (a) Measured SRAPT ratio and (b) fractional temperature sensitivity as a function of temperature for in-situ and furnace measurements.

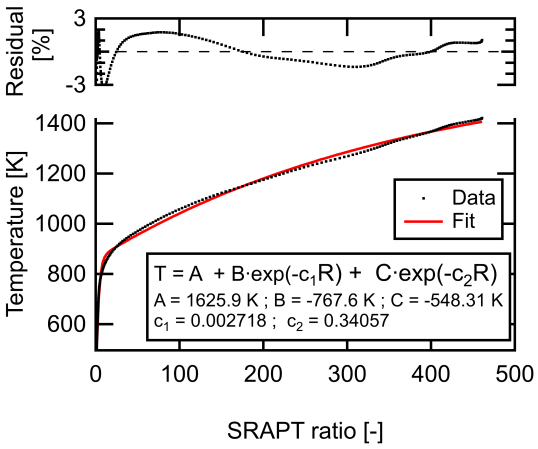

Figure 7: calibration function that is used to translate SRAPT ratio measurements to temperature for the imaging demonstration. Fit residual is shown versus temperature in the top plot.

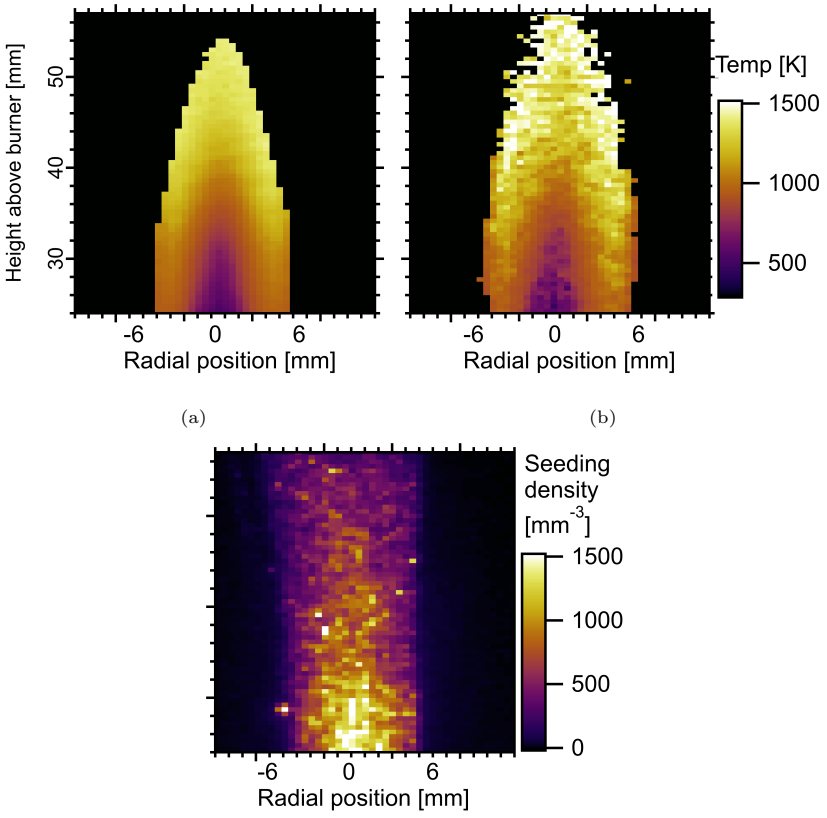

Figure 8: (a) Average temperature measurement, (b) single-shot temperature measurement, and (c) corresponding single-shot seeding density field.

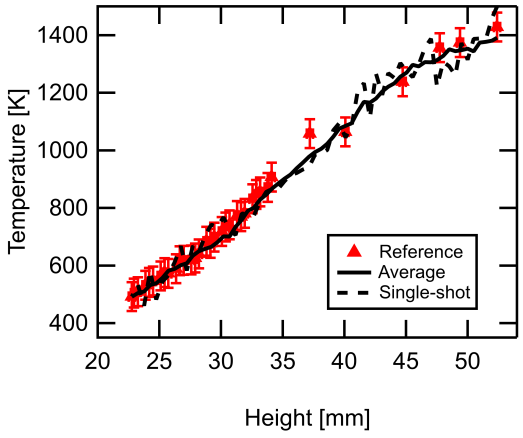

(a)

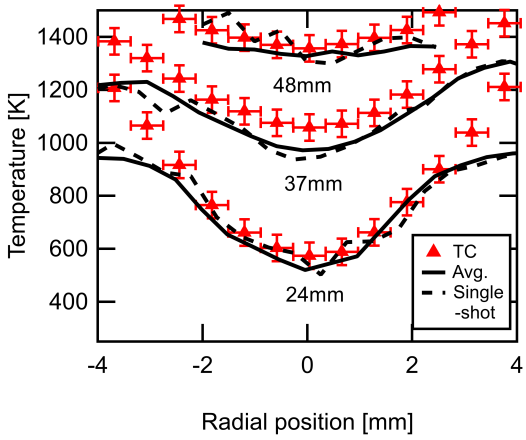

(b)

Figure 9: (a) Comparison of axial temperature profile along the center of the jet between Eu:BAM SRAPT measurements and reference measurements. The reference measurements consist of the Ce,Pr:LuAG measurements at T<1000 K and type-R thermocouple measurements for T>1000 K that were used for the in-situ calibration.(b) Comparison of radial temperature profiles measured by thermocouple and SRAPT at three different heights in the jet.